Internal Report Nr 95/12

CHALMERS TEKNISKA HÖGSKOLA
Institutionen för Termo- och Fluiddynamik

CHALMERS UNIVERSITY OF TECHNOLOGY
Department of Thermo- and Fluid Dynamics

Reynolds Stress Modeling of Flow Separation on Curved Surfaces. A Status Report

by

Sven Perzon, Lars Davidson & Mats Ramnefors
Thermo and Fluid Dynamics
Chalmers University of Technology
412 96 Gothenburg, Sweden

Volvo Data AB
405 08 Gothenburg
Sweden

Göteborg, April 1995

Reynolds Stress Modeling of Flow Separation on Curved Surfaces. A Status Report

by

Sven Perzon[♣] , Lars Davidson[♣] and Mats Ramnefors[♣♣]

[♣]Thermo and Fluid Dynamics
Chalmers University of Technology
412 96 Gothenburg
SWEDEN

[♣♣]Volvo Data AB
2620 CAE
405 08 Gothenburg
SWEDEN

Contents

List of Figures

1 Introduction

When simulating almost any external flow of technical interest there is a curved boundary present. The curvature is important regarding to boundary layer development and turbulence. Some of the turbulence models available in CFD codes today poorly predicts these curvature effects. Two equation models, e.g. k-ε-models, will predict the effects incorrectly. Second order closures, e.g. Reynolds Stress Models (RSM), do account for streamline curvature and should model the turbulence more accurate under these circumstances. However even using RSM, the location of for instance the separation point is not accurate enough which in turn significantly affects the accuracy when estimating the overall drag on cars. The aim for this project is thus to increase the understanding of how turbulence models perform in advanced industrial like flows including separation and high streamline curvatures. Additional models have been and will be implemented in the commercial CFD code, CFDS-FLOW3D. Evaluation are taken place in common with Volvo Data where the implemented models will be tested in an industrial environment. This is a status report that shows what has been done so far in this NUTEK project, which was started July 1, 1994. Some conclusions will be made about the present and future work.

2 The software

The commercial code, CFDS-FLOW3D [1] is used for the computations. It is a general three-dimensional finite volume computer program using body fitted coordinates for three-dimensional complex geometries. The program uses Cartesian velocity components, and the pressure-velocity coupling is handled with a SIMPLEC algorithm. A non-staggered grid arrangement is used, which means that velocities are stored along with all scalar variables like p, k, ε etc. at the center of the control volume.

Collaboration with Harwell Laboratories, the originator of the code, has been initiated through a visit last autumn. Part of the source code has been made available for use in the project.

ICEM-CFD is used for mesh generation and for the linkage between CFDS-FLOW3D and ICEM-CFD, some software has been developed at Volvo Data.

3 Selection of test cases.

For the investigations that was to be done some test cases should be used. They should preferably be in two dimensions in order to save CPU time and make it possible to, in each test case, use different grids and different turbulence models. The project is a collaboration with Volvo Data and thus, the test cases should be related to external flows around cars. Since the aim of the project is to increase the accuracy in the estimation of where the separation point (or line) is located, separation should also occur in the test case at a gently curved surface. In order to detect possible bugs in the implementations, the simple

plane channel flow of Laufer (1952) [11] has been simulated in the initial stages of the coding. Two other test cases have been selected so far and these are described separately below.

4 The axisymmetric body.

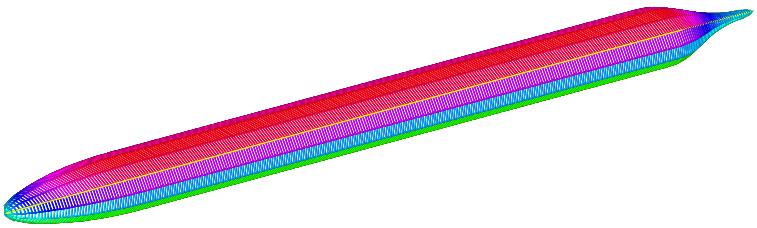

An axisymmetric body with a smooth rear end was choosen as a first test case. Experimental data is present, Huang *et al.*, (1980) [12], at two Reynolds numbers namely: $Re_L = 5.9 \cdot 10^6$ and $Re_L = 8.8 \cdot 10^6$. We computed this test case before any of the source code was available and three different turbulence models were used. These are the commonly used and already implemented k-ε-model, a low Reynolds number k-ε-model and a standard Reynold stress model (RSM). Since there is most experimental data at $Re_L = 5.9 \cdot 10^6$, the computations have been focused on this.

4.1 Turbulence models

As stated above three turbulens models were used in the computations. The standard k-ε-model is one of those and needs no further explanation. See for instance [1].

4.1.1 Low Reynolds number k-ε-model.

The low-Re k-ε-model used is the model by Launder and Sharma [3], hereafter denoted as the 'LS'-model, where a modified definition of the rate of dissipation $\tilde{\varepsilon}$, that goes to zero at walls, is used.

$$\tilde{\varepsilon} = \varepsilon - 2\nu \left(\frac{\partial \sqrt{k}}{\partial x_n} \right)^2$$

where the n index denotes the direction normal to the wall. The equations then become,

$$\frac{\partial}{\partial t}(\rho k) + \mathrm{div}(\rho \vec{U} k) = \mathrm{div}\left((\mu + \frac{\mu_t}{\sigma_k}) \nabla k \right) + P_k - \rho \tilde{\varepsilon} - D \tag{1}$$

$$\frac{\partial}{\partial t}(\rho \tilde{\varepsilon}) + \mathrm{div}(\rho \vec{U} \tilde{\varepsilon}) = \mathrm{div}((\mu + \frac{\mu_t}{\sigma_\varepsilon}) \nabla \tilde{\varepsilon}) + \frac{\tilde{\varepsilon}}{k}(C_1 P_k - C_2 f_2 \rho \tilde{\varepsilon}) + E \tag{2}$$

and the production terms P_k, D and E have the form:

$$P_k = \mu_t \nabla \vec{U} \cdot \left(\nabla \vec{U} + (\nabla \vec{U})^T \right)$$

$$D = 2\mu \left(\nabla\sqrt{k}\right)^2 \quad , \quad E = 2\frac{\mu\mu_t}{\rho}(\nabla\nabla\vec{U})^2$$

where μ_t is,

$$\mu_t = C_\mu f_\mu \frac{\rho k^2}{\tilde{\varepsilon}}$$

and the damping functions,

$$f_\mu = e^{-\frac{3.4}{(1+R_T/50)^2}} \quad \text{and} \quad f_2 = 1 - 0.3e^{-R_T^2}$$

where the local turbulent Reynolds number is defined by $R_T = \rho k^2/(\mu\varepsilon)$.

4.1.2 Second moment closure

For an incompressible turbulent flow, the transport of Reynolds stress tensor, $\overline{u_i u_j}$, can be expressed in a symbolic form as,

$$\frac{\partial}{\partial t}\left(\rho\overline{u_i u_j}\right) + \frac{\partial}{\partial x_k}\left(\rho U_k \overline{u_i u_j}\right) = P_{ij} + D_{ij} + T_{ij} + \Phi_{ij} - \varepsilon_{ij} \tag{3}$$

where the terms can be interpreted as production,

$$P_{ij} = -\left(\rho\overline{u_j u_k}\frac{\partial U_i}{\partial x_k} + \rho\overline{u_i u_k}\frac{\partial U_j}{\partial x_k}\right)$$

viscous diffusion,

$$D_{ij} = \mu\frac{\partial^2\overline{u_i u_j}}{\partial x_k \partial x_k}$$

turbulent diffusion,

$$T_{ij} = -\frac{\partial}{\partial x_k}\left(\rho\overline{u_i u_j u_k} + \overline{pu_j}\delta_{ik} + \overline{pu_i}\delta_{jk}\right)$$

pressure strain interaction,

$$\Phi_{ij} = \overline{p\left(\frac{\partial u_i}{\partial x_j} + \frac{\partial u_j}{\partial x_i}\right)}$$

and finally dissipation,

$$\varepsilon_{ij} = 2\mu\overline{\frac{\partial u_i}{\partial x_k}\frac{\partial u_j}{\partial x_k}}$$

Of these terms the turbulent diffusion, the pressure strain interaction and the dissipation terms have to be modelled. In CFDS-FLOW3D the turbulent diffusion term is modelled using the generalized gradient diffusion hypothesis (GGDH) of Daly and Harlow [15].

$$T_{ij} = \frac{\partial}{\partial x_k}\left(c_s\frac{k}{\varepsilon}\overline{u_k u_l}\frac{\partial\overline{u_i u_j}}{\partial x_l}\right) \tag{4}$$

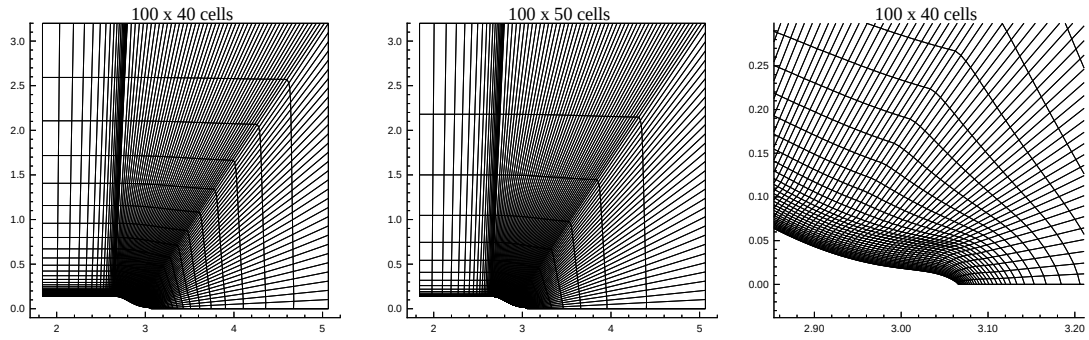

Figure 1: *A* **100x40** *mesh made for wall functions and a* **100x50** *mesh made for use with the low Re k-ε-model. The last picture is an enlargement of the region of the rear end.*

Furthermore the pressure strain interaction term is modelled using a common and simple linear proposal based upon the slow pressure strain term by Rotta [7] and the rapid pressure strain term by Naot *et al.* [6].

$$\Phi_{ij} = \underbrace{-c_1\rho\frac{\varepsilon}{k}\left(\overline{u_iu_j} - \frac{2}{3}\delta_{ij}k\right)}_{\Phi_{ij,1}} \underbrace{-c_2\left(P_{ij} - \frac{2}{3}\delta_{ij}P\right)}_{\Phi_{ij,2}} + \Phi_{ij,w} \tag{5}$$

where $P = \frac{1}{2}P_{ii}$ and the wall reflection term is expressed according to Gibson and Launder [8] as,

$$\begin{aligned}\Phi_{ij,w} \quad = \quad & \left(c_1'\frac{\varepsilon}{k}\rho\left(\overline{u_ku_m}\hat{n}_k\hat{n}_m\delta_{ij} - \tfrac{3}{2}\overline{u_ku_i}\hat{n}_k\hat{n}_j - \tfrac{3}{2}\overline{u_ku_j}\hat{n}_k\hat{n}_i\right)\right. \\ & \left. +c_2'\left(\Phi_{km,2}\hat{n}_k\hat{n}_m\delta_{ij} - \tfrac{3}{2}\Phi_{ik,2}\hat{n}_k\hat{n}_j - \tfrac{3}{2}\Phi_{jk,2}\hat{n}_k\hat{n}_i\right)\right) f\end{aligned} \tag{6}$$

The wall damping function, f, is defined as $f = c_\mu^{3/4}k^{3/2}/\kappa\eta\varepsilon$ where η is the normal distance to the wall and $\vec{n} = (\hat{n}_1, \hat{n}_2, \hat{n}_3)$ is the unit normal vector at the wall. $\Phi_{ij,w}$ is difficult to code in a general way and it is excluded by default in CFDS-FLOW3D, see [1]. The model is described thoroughly in [2]. The dissipation term is modelled as $\varepsilon_{ij} = \frac{2}{3}\varepsilon\delta_{ij}$, see [1].

In order to close equation 3, an equation for the rate of dissipation, ε, is needed,

$$\frac{\partial}{\partial t}(\rho\varepsilon) + \frac{\partial}{\partial x_k}(\rho U_k\varepsilon) = \frac{\partial}{\partial x_k}\left(\rho\frac{c_s}{\sigma_\varepsilon}\frac{k}{\varepsilon}\overline{u_ku_l}\frac{\partial\varepsilon}{\partial x_l}\right) + \frac{\varepsilon}{k}\left(c_{\varepsilon1}P - c_{\varepsilon2}\rho\varepsilon\right) \tag{7}$$

4.2 The mesh

The grids used in the computations are a one block structured mesh consisting of **100x40** cells for the two high Reynolds number models and **100x50** cells for the low Reynolds number model, see figure 1. The center of the innermost cell was located at a distance $y^+ = 20$ and $y^+ = 0.1$ respectively.

4.3 Boundary conditions

Inlet conditions where obtained using the results from a previous computation of a circular channel. The reasoning was as follows. Homogeneous profile where set to U according to the Reynolds number in the experiments. The V velocity was of course set to zero and turbulent quantities were set to low positive values except for the $\overline{uv}$-stress, which was set to zero. The plane channel flow was computed and a profile from this computation was about to be selected. The inlet was chosen to be at $x/L = 0.6$ where only the skin friction coefficient was available from measurement. Thus the inlet profiles of all variables could be taken where the channel flow reached this skin friction coefficient.

Outlet conditions where set as homogeneous Neuman conditions for all variables.

At the walls wall functions are used for the high Reynolds number models and for the low Reynolds number model a homogeneous Dirichlet boundary condition is applied on all variables, see [1].

4.4 Convection schemes

The Higher-order upwind, (HUW), (see Ref. [1]) is used for all variables except for the Reynolds stresses in the differential stress model where the first order accurate Hybrid scheme was used. This was due to stability problems.

4.5 Results

A small separation bubble is present in experiments at $x/L = 0.918$ but in the computations no separation occured. As a criterion of separation one could use the sign of the friction coefficient, c_f, and as can be seen in figure 2 the RSM is closer to separation than the k-ε-model. The pressure distribution along the surface of the body are shown in figure 3 and computations comply well for all models except at what should be the separated region where the RSM proves to be more accurate than the standard k-ε-model. The low Reynolds number k-ε-model did not give any results since no convergence was reached. This is due to the fact that during iterations the solution oscillates between two steady state solutions, separated and not. In the computations using the low Reynolds number k-ε-model and $Re_L = 8.8 \cdot 10^6$ a stable solution is reached and separation occurs at $x/L = 0.912$, see figure 4. The high Reynolds number models did not separate for this Reynolds number.

4.6 Conclusions

We can conclude that RSM does work better than the k-ε-model and that wall functions do not work very well when it comes to separation. Approaching the separation point, wall functions are not valid anymore and thus give rise to discrepancies. The low Re k-ε-model seems to work even better than the RSM and the flow separates[1] using this

[1] At $Re_L = 8.8 \cdot 10^6$.

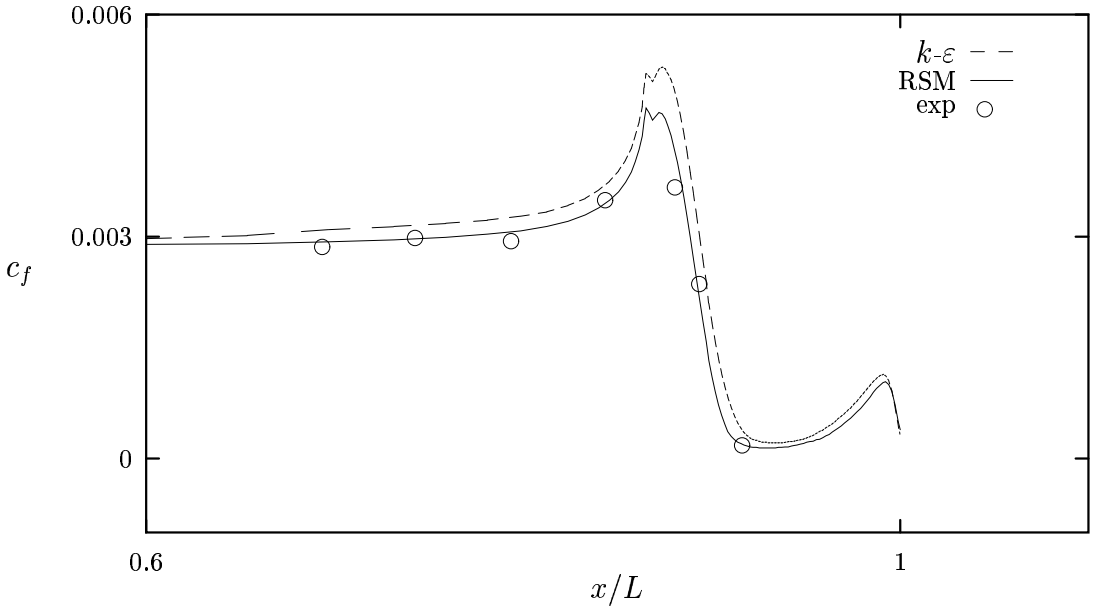

Figure 2: c_f *at* $Re_L = 5.9 \cdot 10^6$.

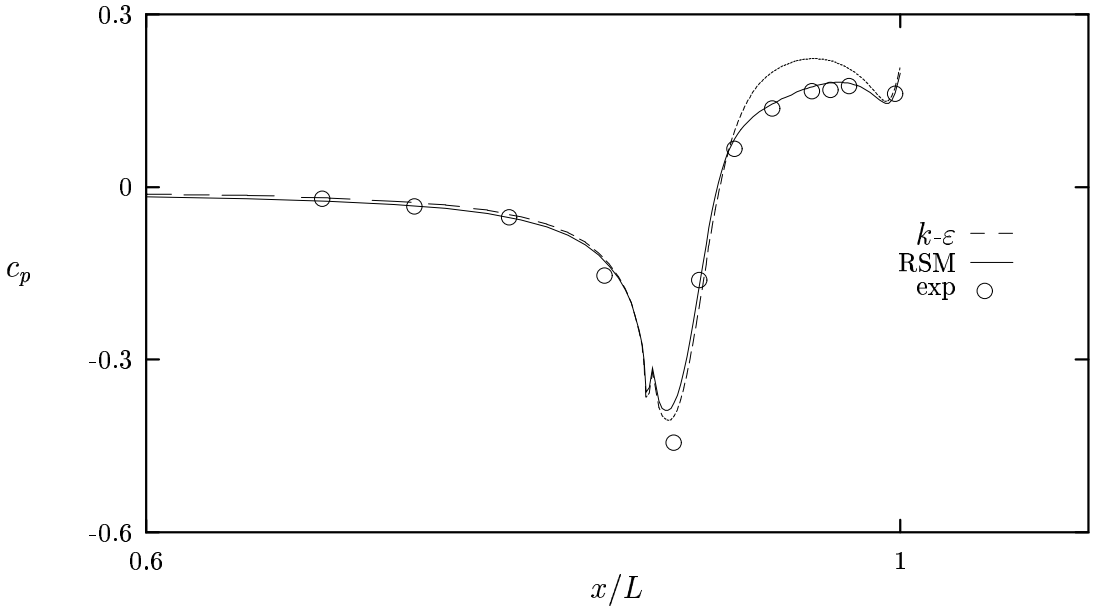

Figure 3: c_p *at* $Re_L = 5.9 \cdot 10^6$.

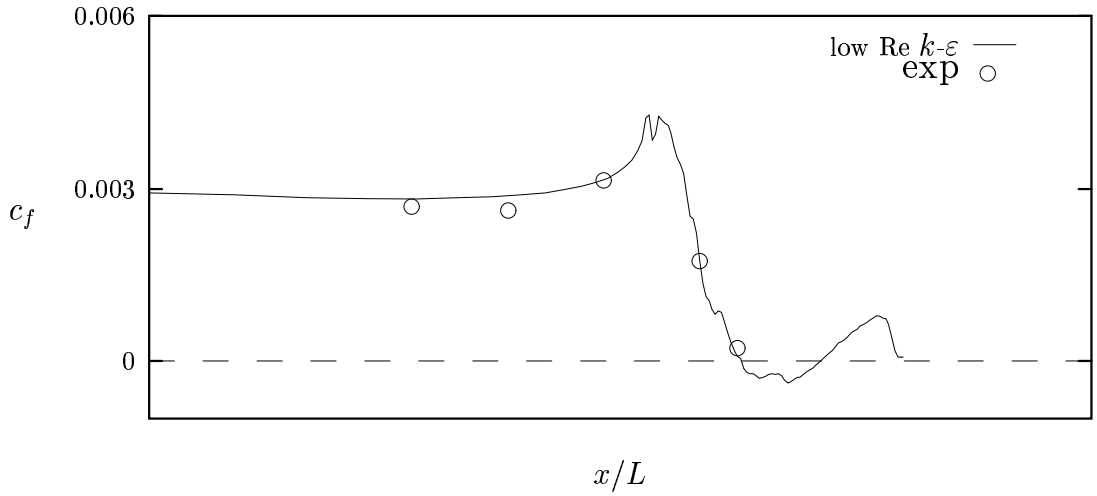

Figure 4: c_f *at* $Re_L = 8.8 \cdot 10^6$.

model which does not happen using any other model. However, this comparison is not very valid since the RSM was wall-function-based. A more interesting comparison should be to test this low-Re k-ε-model versus some low-Re RSM.

Wall reflection terms in the pressure-strain term are excluded by default in CFDS-FLOW3D. This is because it is almost impossible to implement these terms in a general way. This fact is also a source of discrepancies in wall bounded flows and should be investigated more properly.

Another important note is that the experimental data is not very extensive. In order to compare turbulence models one must have access to measurement of turbulent quantities like the Reynolds stresses and the turbulent kinetic energy, k. Therefore another test case is necessary.

5 2D hill flows

The next test case is chosen to be the flow over a 2D hill, see figure 5, which is a test case within the ERCOFTAC/IAHR *Workshop on Databases and Testing of Calculation Methods for Turbulent Flows*, April 3-7, University of Karlsruhe where these results were presented. This test case has been measured by Almeida *et al.* [10] and an extensive amount of flow quantities are available including turbulent quantities.

5.1 Flow description

The domain is shown in figure 5 and the geometrical parameters are,

- Channel height, $H = 170$ mm
- Hill height, $h = 28$ mm

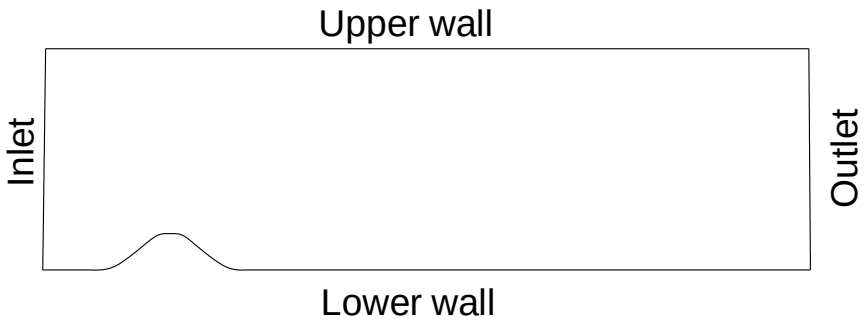

Figure 5: *Domain for 2D hill flow.*

The top of the hill should be located 100 mm after the inlet and the outlet should be placed sufficiently far downstream. Furthermore flow parameters are (water),

- Density, $\rho = 1000$ kg/m^3
- Kinematic viscosity, $\nu = 1 \cdot 10^{-6}$ m^2/s
- Mean centerline velocity at the inlet, $U_0 = 2.147$ m/s

This gives a Reynolds number,

$$Re_h = \frac{U_0 h}{\nu} = 60\,000$$

5.2 The mesh

The grids used were created using the ICEM-CFD mesh generator. The grid size for the different near-wall treatments are,

- Wall function models: **122 x 50** see figure 6
- Low Reynolds number models: **128 x 100** see figure 7

5.3 Turbulence models

5.3.1 Two equation models

The standard k-ε-model has been used together with the low Reynolds number formulation of the model described in section 4.1.1.

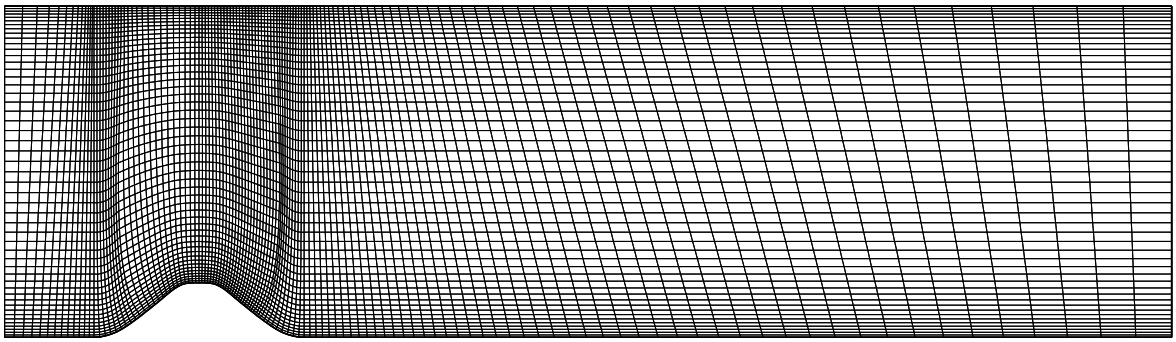

Figure 6: *Grid with 122x50 cells for 2D hill flow.*

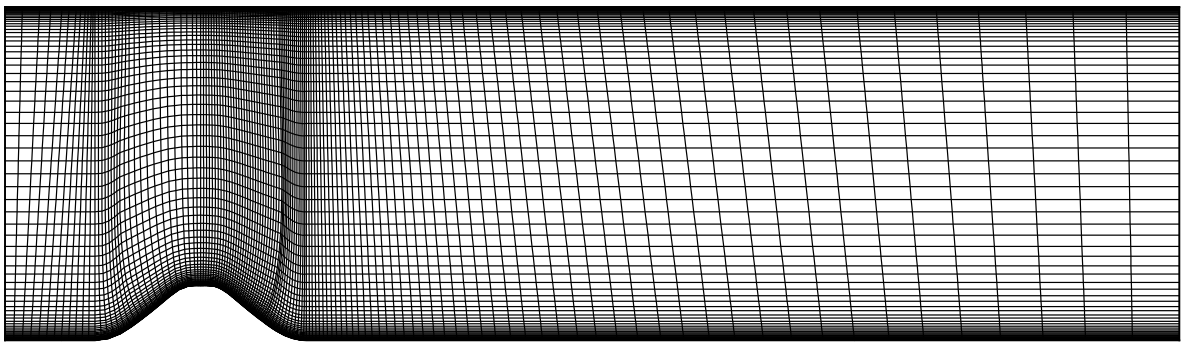

Figure 7: *Grid with 128x100 cells for 2D hill flow.*

5.3.2 Reynolds Stress Models

The differential stress model is described in section 4.1.2. Two high Reynolds number models have been used and these differ only by different pressure strain interaction terms where the default linear model is mentioned earlier, e.g. equation (5), hereby denoted by 'RSM'. A nonlinear proposal for the presure strain interaction term has been developed by Speziale *et al.* [9],

$$\begin{aligned}\Phi_{ij} &= - \left(c_1\varepsilon + c_1^* P\right) b_{ij} + c_2\varepsilon \left(b_{ik}b_{kj} - \tfrac{1}{3}b_{kl}b_{kl}\delta_{ij}\right) \\ &+ kS_{ij}\left(c_3 - c_3^*\sqrt{\mathrm{II}}\right) + c_4 k \left(b_{ik}S_{jk} + b_{jk}S_{ik} - \tfrac{2}{3}b_{kl}S_{kl}\delta_{ij}\right) \\ &+ c_5 k \left(b_{ik}\Omega_{jk} + b_{jk}\Omega_{ik}\right)\end{aligned} \tag{8}$$

where

$$S_{ij} = \tfrac{1}{2}\left(\tfrac{\partial U_i}{\partial x_j} + \tfrac{\partial U_j}{\partial x_i}\right), \quad \Omega_{ij} = \tfrac{1}{2}\left(\tfrac{\partial U_i}{\partial x_j} - \tfrac{\partial U_j}{\partial x_i}\right)$$

$$b_{ij} = \tfrac{\overline{u_iu_j} - \frac{2}{3}k\delta_{ij}}{2k}, \qquad \mathrm{II} = b_{ij}b_{ji}$$

and the constants should take the following values: $c_1 = 3.4$, $c_1^* = 1.8$, $c_2 = 4.2$, $c_3 = 0.8$, $c_3^* = 1.3$, $c_4 = 1.25$ and $c_5 = 0.4$. This model, hereafter called the 'SSG'-model, does not include any wall reflection terms.

Besides these models a low Reynolds number model have been used. It is the model of Hanjalić and Launder [5] and it is hereby named as the 'HL'-model. The HL-model starts off as the other two differential stress models with equation (3) but models the pressure strain interaction term, the turbulent diffusion term and the dissipation term differently from previously described models.

HL-model does not use the GGDH for the turbulent diffusion but model the diffusion using a more complex proposal that **does** satisfy coordinate invariance,

$$\overline{u_iu_ju_k} = -c_s\frac{k}{\varepsilon}\left(\overline{u_iu_l}\frac{\partial\overline{u_ju_k}}{\partial x_l} + \overline{u_ju_l}\frac{\partial\overline{u_iu_k}}{\partial x_l} + \overline{u_ku_l}\frac{\partial\overline{u_iu_j}}{\partial x_l}\right) \tag{9}$$

The GGDH does not fulfill this coordinate invariance requirement. The present calculations are carried out using the GGDH and this is due to the fact that this part of the source code was not available at the time of the computations. It has recently arrived which means that the results can and will be followed up using the correct diffusion model. In order to see whether or not the choice of diffusion model gives reasonable results when used in the HL-model can be shown in the simple test case, the plane channel flow of Laufer [11] which was used for debugging purposes, see figure 13 in appendix.

The pressure strain interaction term is modelled using the high Reynolds number variant proposed in Launder *et al.* [4]. It is a linear model with a slightly more advanced

rapid part, (eg. $\Phi_{ij,2}$), and the model is,

$$\begin{aligned}\Phi_{ij} &= \underbrace{-c_1\rho\frac{\varepsilon}{k}\left(\overline{u_iu_j}-\frac{2}{3}\delta_{ij}k\right)}_{\Phi_{ij,1}} \\ &\underbrace{-\frac{(c_2+8)}{11}\left(P_{ij}-\frac{2}{3}\delta_{ij}P\right)-\frac{60c_2-4}{55}S_{ij}-\frac{8c_2-2}{11}\left(\mathcal{D}_{ij}-\frac{2}{3}\delta_{ij}P\right)}_{\Phi_{ij,2}} \\ &\underbrace{+\left(0.125\rho\frac{\varepsilon}{k}\left(\overline{u_iu_j}-\frac{2}{3}k\delta_{ij}\right)+0.015\left(P_{ij}-\mathcal{D}_{ij}\right)\right)\frac{k^{3/2}}{\varepsilon\eta}}_{\Phi_{ij,w}}\end{aligned} \tag{10}$$

where η is the normal distance to the wall and,

$$\mathcal{D}_{ij} = -\left(\rho\overline{u_iu_k}\frac{\partial U_k}{\partial x_j}+\rho\overline{u_ju_k}\frac{\partial U_k}{\partial x_i}\right)$$

c_1 and c_2 are model constants and takes the values 1.5 and 0.4 respectively.

Furthermore the dissipation term is modelled as,

$$\varepsilon_{ij} = \frac{2}{3}\varepsilon\left((1-f_s)\delta_{ij}+\frac{\overline{u_iu_j}}{2k/3}f_s\right) \tag{11}$$

where the dampfunction is chosen as $f_s = (1+R_T/10)^{-1}$, see [5]. Modifications are also introduced in the dissipation equation which in this low Reynolds number proposal has the form,

$$\begin{aligned}\frac{\partial}{\partial t}(\rho\varepsilon)+\frac{\partial}{\partial x_k}(\rho U_k\varepsilon) &= \frac{\partial}{\partial x_k}\left(\mu\frac{\partial\varepsilon}{\partial x_l}+\rho\frac{c_s}{\sigma_\varepsilon}\frac{k}{\varepsilon}\overline{u_ku_l}\frac{\partial\varepsilon}{\partial x_l}\right)+\frac{\varepsilon}{k}\left(c_{\varepsilon1}P-c_{\varepsilon2}f_\varepsilon\rho\tilde{\varepsilon}\right) \\ &\quad +c_{\varepsilon3}\mu\frac{k}{\varepsilon}\overline{u_ju_k}\frac{\partial^2U_i}{\partial x_j\partial x_l}\frac{\partial^2U_i}{\partial x_k\partial x_l}\end{aligned} \tag{12}$$

where $\tilde{\varepsilon}$ is defined as

$$\tilde{\varepsilon} = \varepsilon - 2\nu\left(\frac{\partial\sqrt{k}}{\partial x_n}\right)^2$$

and the dampfunction is chosen to be

$$f_\varepsilon = 1-\frac{0.4}{1.8}e^{-(R_T/6)^2}$$

and the model constants $c_{\varepsilon1}$, $c_{\varepsilon2}$ and $c_{\varepsilon3}$ are assigned the values 1.275, 1.8 and 2.0 respectively, see [5].

5.4 Boundary conditions

Inlet boundary conditions were obtained using measurements interpolated linearly to the gridnodes. Experiments were available for all variables but ε which were set according to the assumption that the production balances dissipation in a fully developed flow, e.g.

$$\varepsilon = -\overline{uv}\frac{\partial U}{\partial y} \tag{13}$$

The validity of this boundary condition for ε was checked using a separate channel flow computation solving only for ε and keeping all other variables according to experiments. The result are compared to the assumed profile described in equation (13), see figure 14 in appendix. Outlet conditions were set to homogeneous Neuman conditions for all variables.

At the walls wall functions are used for the high Reynolds number models and for the low Reynolds number k-ε-model a homogeneous Dirichlet boundary condition is applied on all variables, see [1]. For the HL-model a homogeneous Dirichlet boundary condition is applied on all variables but ε which was set to,

$$\varepsilon = 2\nu\left(\frac{\partial\sqrt{k}}{\partial x_n}\right)^2$$

at the wall. Index n denotes the normal direction to the wall.

5.5 Convection schemes

The QUICK-scheme is used for mean velocities, Higher order upwind scheme (HUW) is used for k and ε. The Reynolds stresses, in the differential stress models, were solved using the first order accurate Hybrid scheme. This was due to stability problems. For a description of the schemes se for instance Ref. [1].

5.6 Results, 2D Hill Flow

The location for the separation point is estimated to about $x_s = 0.012$ m after the hill-top in the experiments, see [10]. Furthermore the reattachment point is located at about 0.135 m after the top of the hill that is $x/h = 4.8214$.

This test case even increased the necessity for better near-wall models discussed in section 4.6. Wall function based models completely fails in capturing the separation point and the separation is way too late and thus the separated area becomes too small, see figure 8. On the other hand a more advanced pressure strain interaction term, e.g. the SSG-model see figure 9, shows that improvement can be made by just using a better turbulence model but still the separation region is too small. The low Reynolds number k-ε-model shows better agreement with experiments even though the separation area is overpredicted in the first part of the bubble. The bubble recovers fast and the reattachment point is accurately predicted. This means that the height of the separation region is overpredicted

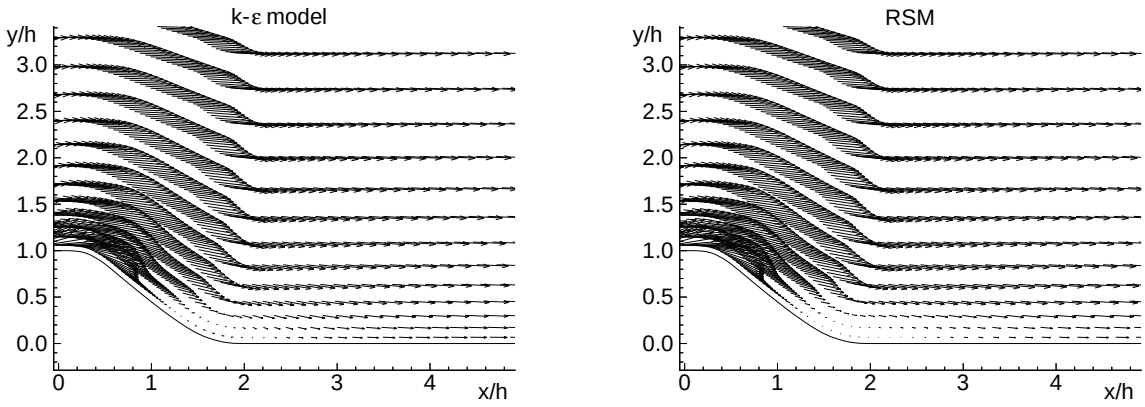

Figure 8: *Velocity vectors showing the separated region using the k-ε-model and the RSM respectively.*

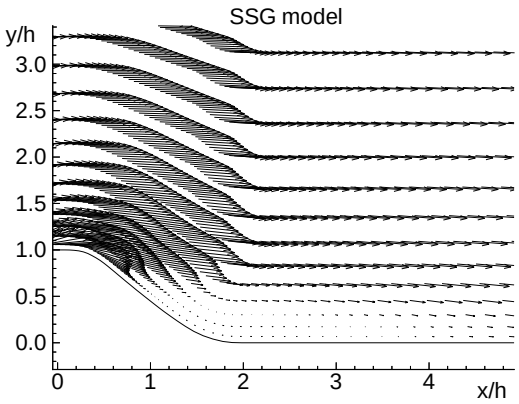

Figure 9: *Velocity vectors showing the separated region using the SSG model.*

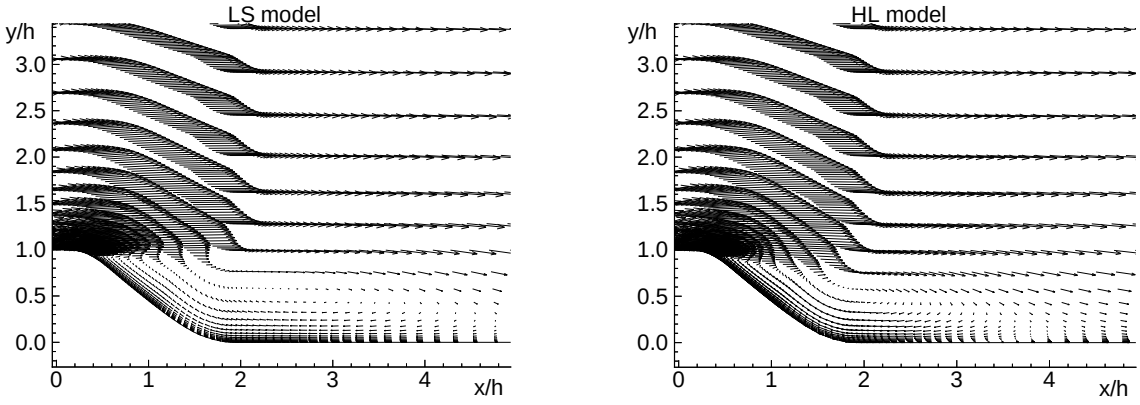

Figure 10: *Velocity vectors showing the separated region using the LS-model and the HL-model respectively.*

in combination with that the length of it is quite well predicted, see figure 10. The separation occurs at about $x = 0.010$ m which is too early. The HL-model proves to give the best agreement with experiments in predicting the separation point at $x = 0.015$ m, see figure 10. This model predicts thus the bubble height correctly and then recovers too fast, rendering too a short separation bubble. The reattachment is therefore too early, see figures 15 and 16 in appendix for a comparison of the mean flow with expriments. Furthermore all high Reynolds number models tested show large discrepancies for the turbulent quantities in the separated region. This is of course due to the fact that the error that occurs when the location of the separation point is predicted poorly the separation bubble becomes too small. This is then convected downstream with large discrepancies for the mean velocity and naturally also for turbulent quantities as a consequence, see figures 17 and 18. The low Reynolds number models are much more accurate in this region. However the LS-model is overpredicting the turbulent kinetic energy at the top of the hill. This is also the fact with the standard k-ε-model, see figure 17. The reason for this is that the acceleration of the flow over the top or the blockage of the flow is known to create problems with too high production term using k-ε-models. RSMs as the HL-model do account for this phenomena since the production terms in the stress equations are exact. Figure 17 also shows better agreement with experiments for the HL-model compared to the LS-model in the first part of the separated region whereas the LS-model is more accurate in the rear part and in the far wake. This is natural since the flow attached to early using the HL-model and therefore rendering downstream discrepancies. Shear stress profiles are shown in figure 18 for the RSMs and show reasonably good agreement with experiments except for the latter part of the separated region as discussed above.

5.6.1 Curvature effects

It can also be interesting to see how the curvature of the flow affects turbulence in the models. Curvature can be measured by the curvature radius R_c,

$$\frac{1}{R_c} = \left. \frac{d^2y/dx^2}{\left(1 + (dy/dx)^2\right)^{3/2}} \right|_{\psi=\text{const}}$$

$$\text{high curvature radius} \Longleftrightarrow \text{low curvature}$$

With $dy/dx|_{\psi=\text{const}} = V/U$ this equation becomes,

$$\frac{1}{R_c} = \frac{UV\left(\frac{\partial V}{\partial y} - \frac{\partial U}{\partial x}\right) + U^2\frac{\partial V}{\partial x} - V^2\frac{\partial U}{\partial y}}{(U^2 + V^2)^{3/2}} \tag{14}$$

This quantity can graphically be visualized as in figure 11 where the peeks have been cut off at $1/R_c = \pm 50m^{-1}$ in order to make changes visible. This cut-off value is of two orders lower in magnitude than the highest and lowest peek. Budgets of the shear stress equation at the location marked in figure 11 show rapid respons to curvature changes. This is natural but is the respons accurate? The production term is of course correct since it is exact. Therefore it is interesting to see how the modelled terms respond to a large streamline curvature change, see figure 12. At this stage of the work it is too early to say anything about these changes since there is nothing to compare with. However streamline curvature effects are important and present models do not fully describe how this affects turbulence and proposals have been made for curvature corrections, see [16] and [17]. These issues will be investigated more properly within a recent future.

5.7 Conclusions, 2D Hill Flow

The first natural conclusion that emanates from the discussion above is that wall functions are hazardous to use in separated flows. It looks as if it is necessary to resolve the boundary layer including the viscous sublayer. This is of course costly but seems unevitable in advanced flows including separation. It should be noted that there were results presented at the ERCOFTAC Workshop [13] where the standard k-ε-model with wall functions were used and impressive results was given. It is hard to explain why but one reason may be some different approach with the wall functions. Different grids, boundary conditions and convection schemes might also give rise to distinctions between solutions. There is two-layer proposals in the litterature that might solve at least part of the problem with wall functions. However most of these proposals require a resolution that is as fine as what is necessary for low Reynold number models. One model that should not need this mesh resolution is a proposal by Haroutunian and Engelman [14] that allows the first

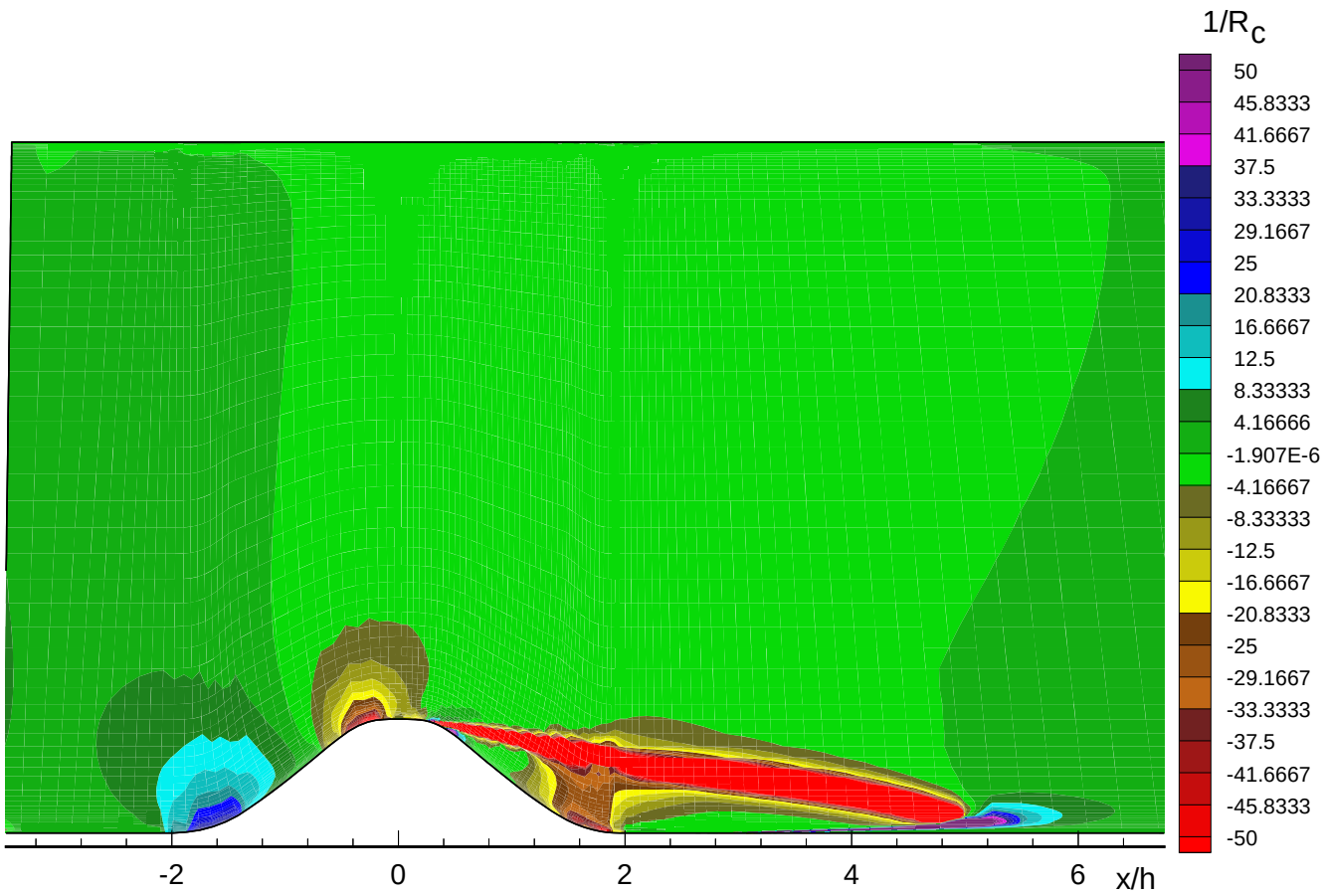

Figure 11: *Streamline curvature isocontours using the HL-model.*

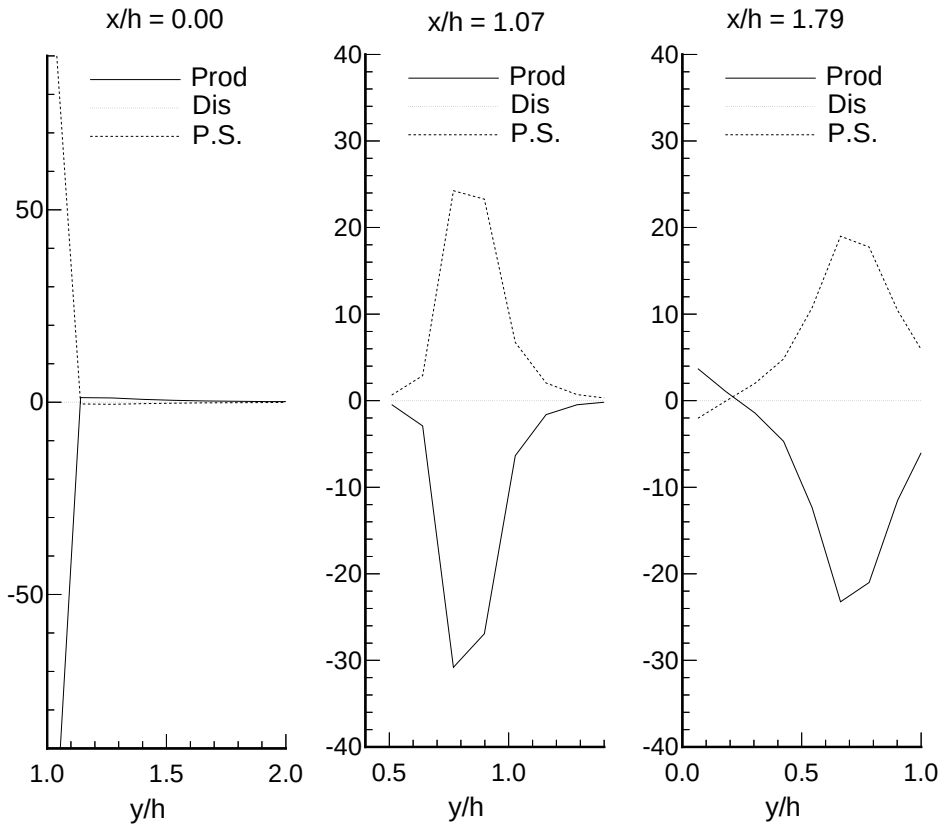

Figure 12: *Parts of $\overline{uv}$ budget at three x-locations using the HL-model. P.S. denotes the pressure strain interaction term.*

grid point to be as far as the initial part of the loglayer from the wall, that is $y^+ \sim 10$. Using this model one would be safe no matter if the first grid node is inside or outside the viscous sublayer and thus it is easier to generate the grid without knowledge about the thickness of the boundary layer.

Furthermore some improvements could be made by using a more advanced pressure strain interaction model, e.g. the SSG-model. This model gave best result among the tested high Reynolds number models. Another benefit gained from this model is that it does not need wall compensation terms which are hard to implement in a general manner.

The low Reynolds number models proved to be much more accurate for this test case. The HL-model predicts the location of the separation point more accurate than the LS-model. Stability problems were present using both models however the for the LS-model these problems were easily solved, adjusting underrelaxation factors. The HL-model was extremely sensitive and unstable and both the stresses and the rate of dissipation ε had to be heavily underrelaxated during the iteration process which in turn lead to many iterations and long computational times. It is not surprising if these convergence problems even increase when problems in 3D are computed. This is of course a major drawback with the HL-model since one of the basic demands that industry has when using CFD is robustness and cost effective codes. Maybe some other low-Re RSM can overcome these difficulties. An other interesting approach might be to use a two-layer RSM which means that a one or two equation model is used in the near wall region and a high-Re RSM is matched with this simple model. Then stability is gained and accuracy is increased compared to using wall functions. The drawback is of course the costly grid resolution of the boundary layer that is necessary together with the difficult coding of the matching line in a general code.

References

[1] CFDS-FLOW3D 3.3 User Guide, AEA Technology, Harwell Laboratory, UK, 1994.

[2] CLARKE, D.S. and WILKES, N.S., The Calculation of Turbulent Flows in Complex Geometries using a Differential Stress Model, AERE-R 13428, 1989.

[3] LAUNDER, B.E. and SHARMA, B.T., Application of the Energy Dissipation Model of Turbulence to the Calculation of Flow Near a Spinning Disc, *Lett. Heat and Mass Transfer* 1, 131-138, 1974.

[4] LAUNDER, B.E., REECE, G.J. and RODI, W., Progress in the Development of a Reynolds-Stress Turbulence Closure,*J. Fluid Mech.*,Vol. 68, 537-566, 1975.

[5] HANJALIĆ, K. and LAUNDER, B.E., Contribution Towards a Reynolds-stress Closure for Low-Reynolds-Number Turbulence, *J. Fluid Mech.*, Vol. 74, 593-610, 1976.

[6] NAOT, D., SHAVIT, A., and WOLFSHTEIN, M., Interactions Between Components of the Turbulent Velocity Correlation Tensor, *Israel J. Techn.,* 8, 259, 1970.

[7] ROTTA, J.C., Statistische Theorie Nichthomogener Turbulenz, *Zeitschrift für Physik*, Vol. 129, 547-572, 1951.

[8] GIBSON, M.M. and LAUNDER, B.E., Ground Effects on Pressure Fluctuations in the Atmospheric Boundary Layer, *J. Fluid Mech.*, Vol. 86, Part 3, pp. 491-511, 1978.

[9] SPEZIALE, C.G., SARKAR, S. and GATSKI, T.B., Modeling the Pressure-Strain Correlation of Turbulence, *J. Fluid Mech.*, Vol 227, 245-272, 1991.

[10] ALMEIDA, M.V., DURAU, D.F.G. and HEITOR, M.V., Wake flows behind two-dimensional hills, *Exp. Thermal and Fluid Science*, 7, 87, 1993.

[11] LAUFER, J., Investigation of Turbulent Flow in a Two-dimensional Channel, Rept. 1053, California Institute of Technology, 1952.

[12] HUANG, T.T.,WANG, H.T., SANTELLI, N. and GROVES, N.C., Propeller/Stern/Boundary Layer Interaction on Axisymmetric Bodies. Theory and Experiment., David W. Taylor Naval Ship Research and Development Center, Ship performance dept., Research and development rept., 1976.

[13] ERCOFTAC/IAHR Workshop on Databases and Testing of Calculation Methods for Turbulent Flows, Proceedings, April 3-7, University of Karlsruhe, 1995.

[14] HAROUTUNIAN and ENGELMAN, On Modeling Wall-Bounded Turbulent Flows Using Specialized Near-Wall Finite Elements and the Standard k-ε-model, Advances in Numerical Simulation of Turbulent Flows, ASME Pub. FED-Vol. 117, 1991.

[15] DALY, B.J. and HARLOW, F.H., Transport equation in turbulence, *Phys. Fluids*, 13, 2634-2649, 1970.

[16] CHUNG,M.K., PARK, S.W, and KIM, K.C., Curvature effect on third-order velocity correlations and its model representation, *Physics of Fluids*, Vol. 30, 626-628, 1987.

[17] PARK, S.B, CHUNG,M.K. and CHOI, D.H., Reynolds-Stress Model Analysis of Turbulent Flow over a Curved Axisymmetric Body,*AIAA Journ.*, Vol. 29, No. 4, 591-594, 1991.

A Appendix

A.1 2D channel flow

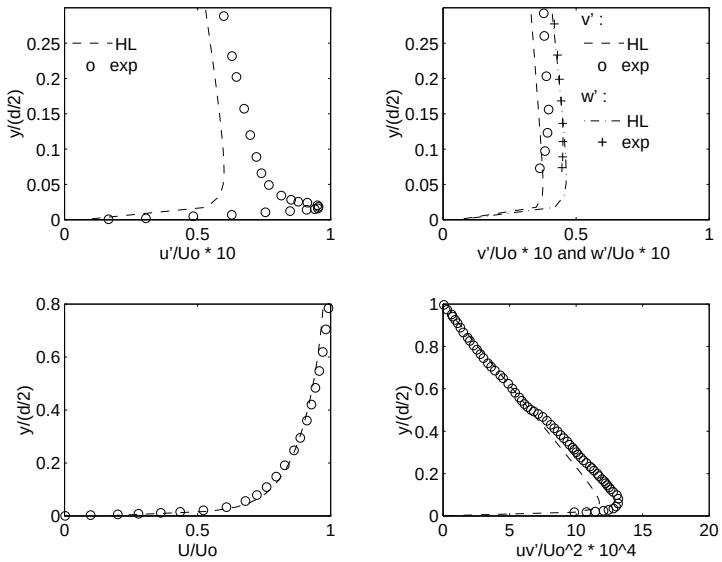

Figure 13: *2D channel flow using HL-model. Experiments from Laufer.*

A.2 Additional figures, 2D hill flow

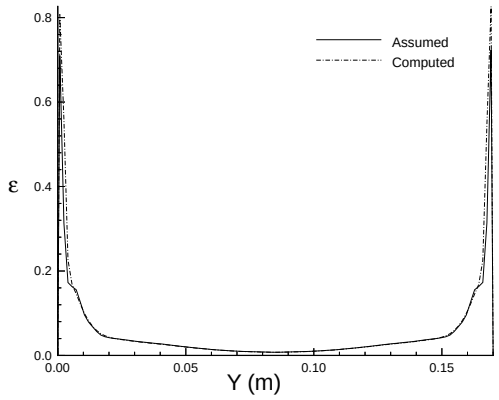

Figure 14: *Comparison between assumed and computed* ε.

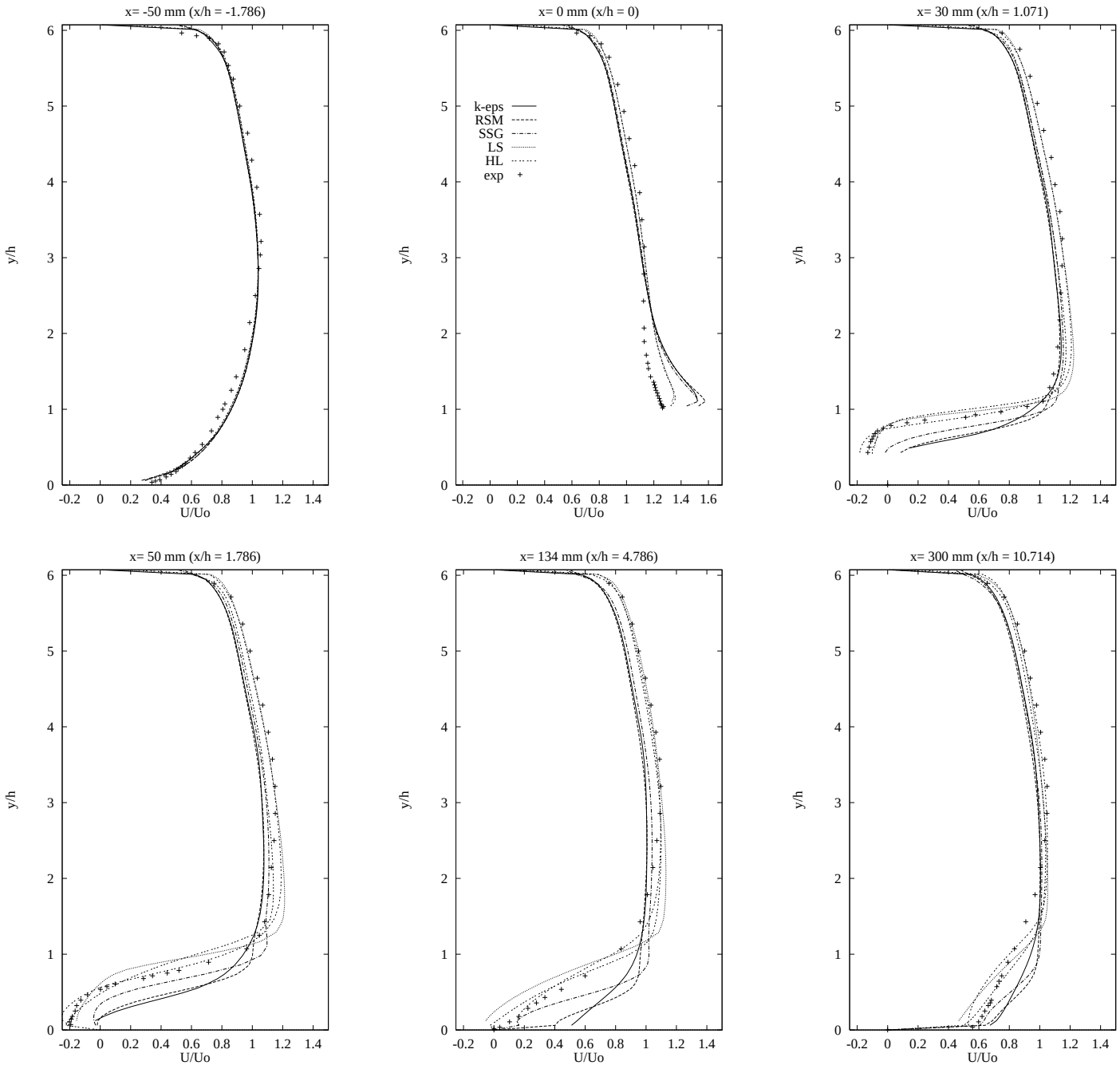

Figure 15: *U velocity profiles at some x-locations.*

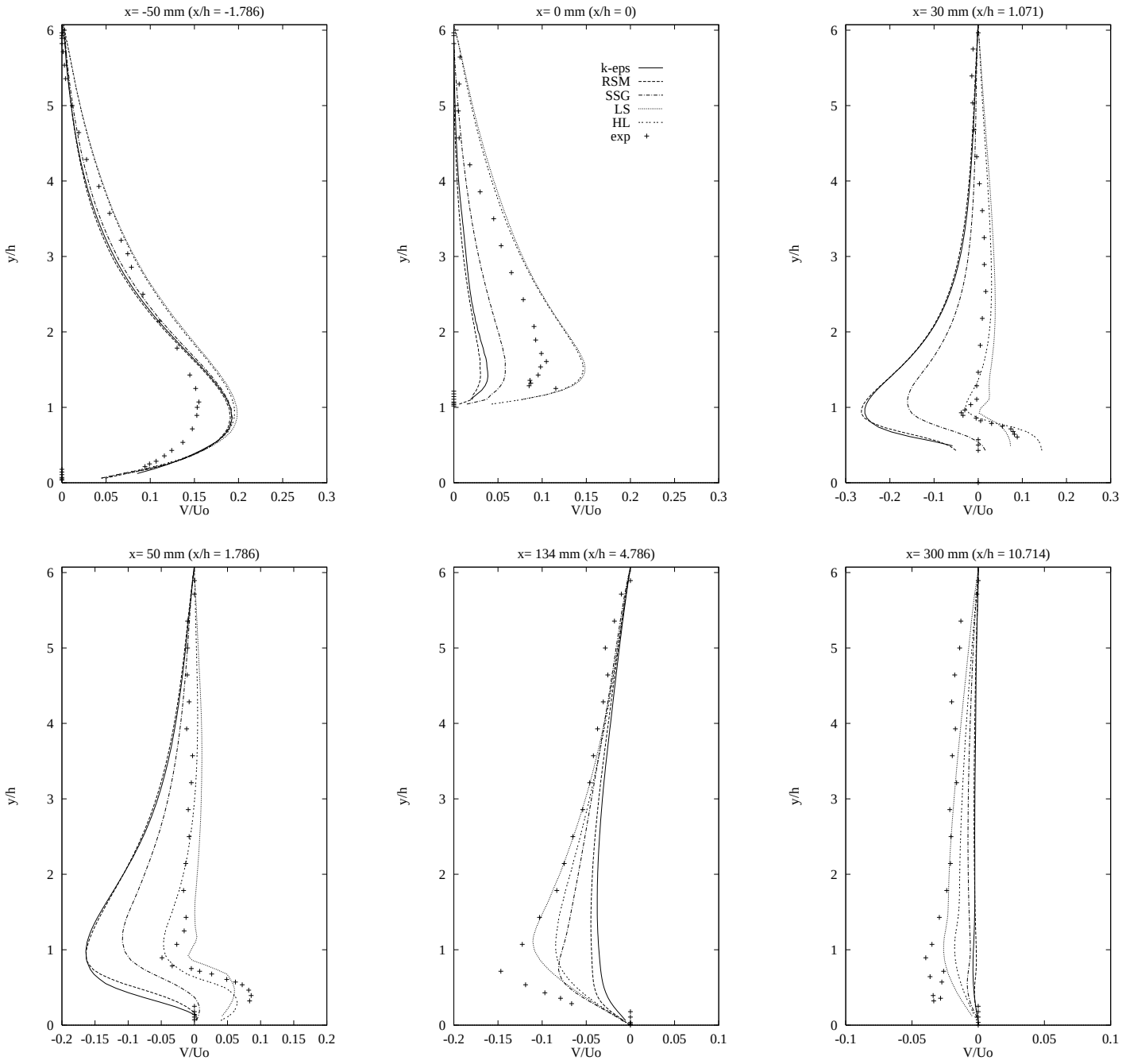

Figure 16: *V velocity profiles at some x-locations.*

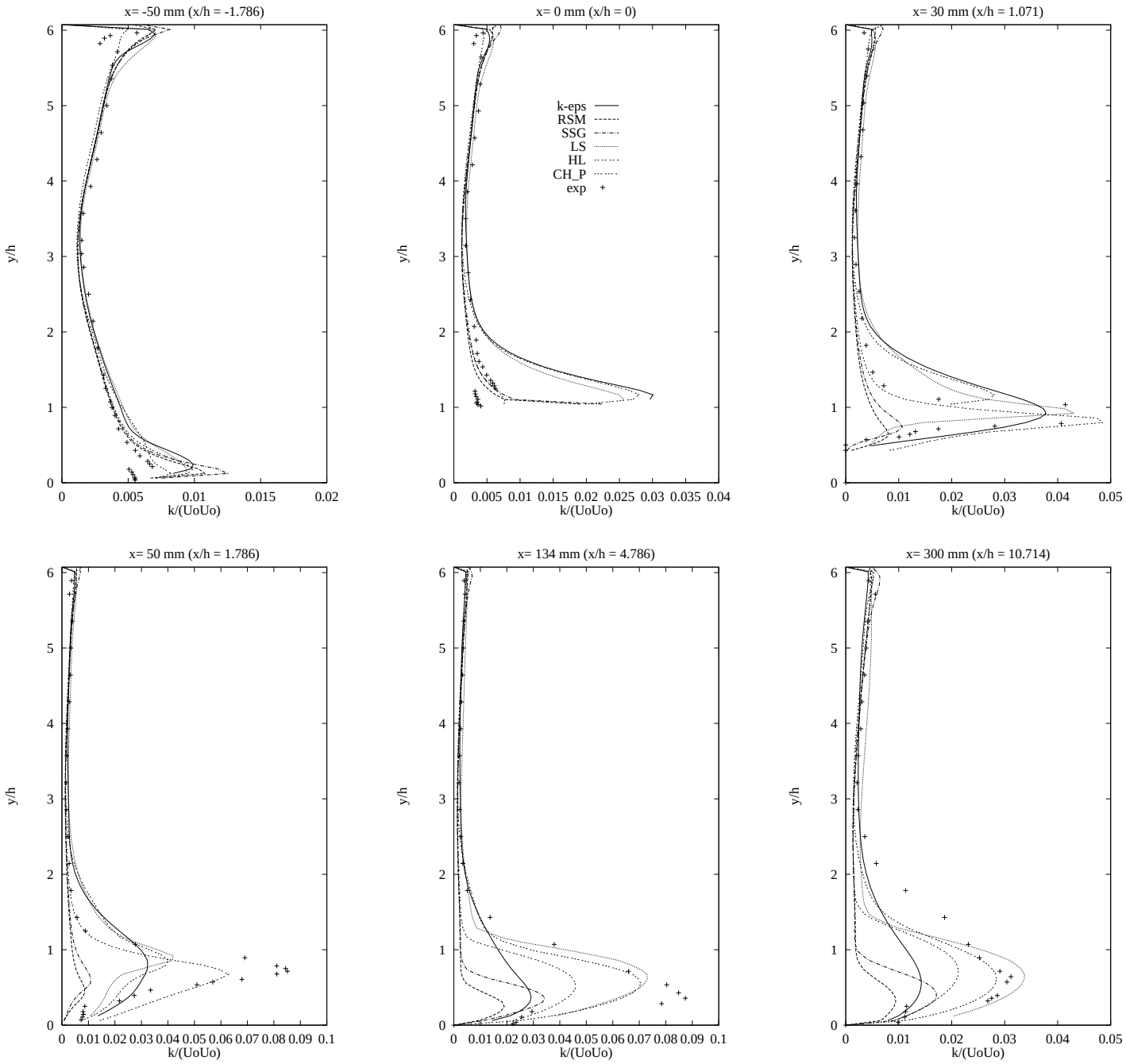

Figure 17: *Turbulent kinetic energy profiles, k, at some x-locations.*

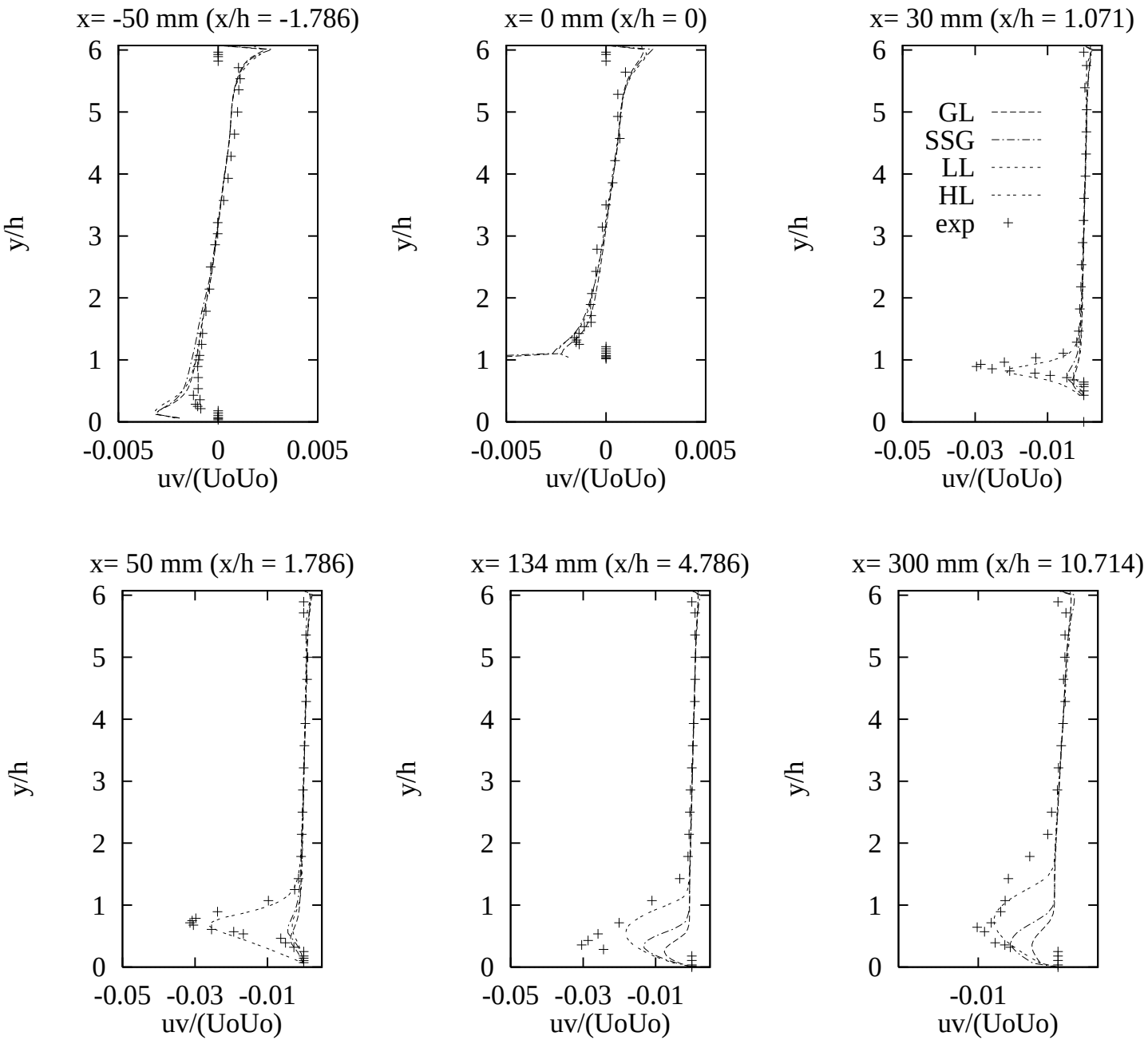

Figure 18: *Shear stress profiles, $\overline{uv}$, at some x-locations.*